Valvular Heart Disease

12

Ludovico La Grutta, Emanuele Grassedonio, Giovanni Gentile, Giuseppe Lo Re, Francesco Coppolino, Giuseppe La Tona, Massimo Galia, and Massimo Midiri

Contents

12.1 Introduction 259

12.2 Anatomy of the Cardiac Valves 260

12.3 Valvular Heart Disease 261
12.3.1 Pathophysiology 261
12.3.2 Echocardiography 263

12.4 Magnetic Resonance Imaging 265
12.4.1 Technique 265
12.4.2 Applications 268

12.5 Computed Tomography 272
12.5.1 Technique 272
12.5.2 Applications 273

References 281

Abbreviations

AR	Aortic regurgitation
AS	Aortic stenosis
CAD	Coronary artery disease
CMR	Cardiac magnetic resonance
CT	Computed tomography
CTCA	Computed tomography coronary angiography
ECG	Electrocardiography
GE	Gradient echo
MR	Mitral regurgitation
MRI	Magnetic resonance imaging
MS	Mitral stenosis
PC	Phase contrast
SSFP	Steady-state free precession
TE	Time of echo
TEE	Transesophageal echocardiography
TI	Time of inversion
TR	Tricuspid regurgitation
TS	Tricuspid stenosis
TTE	Transthoracic echocardiography
VENC	Velocity encoding value
VHD	Valvular heart disease

L. La Grutta • E. Grassedonio • G. Gentile • G. Lo Re
G. La Tona • M. Galia • M. Midiri (✉)
DIBIMEF, Department of Radiology,
University Hospital "P. Giaccone",
Palermo, Italy
e-mail: massimo.midiri@unipa.it

F. Coppolino
Department of Radiology, University Hospital Catania,
Catania, Italy

12.1 Introduction

Valvular heart disease (VHD) is responsible for significant mortality and morbidity worldwide. An estimated 23,313 patients died from VHD in the United States in 2007, with aortic and mitral valve disease accounting for 15,183 and 2,644 deaths, respectively. In 2007, an estimated 98,000

G. Guglielmi et al. (eds.), *Geriatric Imaging*,
DOI 10.1007/978-3-642-35579-0_12,

patients were discharged with a diagnosis of VHD (Roger et al. 2011). According to echocardiographic data, the prevalence of VHD increases with age from 0.7 % in adults from 18 to 44 years to 13.3 % in individuals over 75 years (Nkomo et al. 2006). Cardiac valves are composed of fibromuscular tissue, which may be affected by age-related changes such as myxomatous degeneration, collagen accumulation, sclerosis, and calcification. Common aging phenomena include calcification of the aortic and mitral leaflets and annulus. Aortic stenosis is considered the most frequent indication for valve replacement in elderly individuals (Vahanian et al. 2007; Bonow et al. 2006). Coronary atherosclerosis and aortic calcifications are directly correlated in elderly patients with an increased risk of major cardiac events (Pohle et al. 2001). Hypertension or ischemic heart disease may cause mitral valve regurgitation, while pulmonary hypertension and heart failure can lead to tricuspid or pulmonic regurgitation. Elderly patients may undergo valve replacement with an increased risk of infection and complications (Dauterman et al. 2003).

Echocardiography has been widely deployed for the evaluation of VHD because of its accessibility and cost-effectiveness (Vahanian et al. 2007; Bonow et al. 2006). Three-dimensional techniques such as magnetic resonance imaging (MRI) and computed tomography (CT) have been implemented recently in VHD imaging. MRI could evolve into becoming a reference standard because of its high reproducibility and lack of ionizing radiation exposure. Despite the exposure to radiation, CT may be useful in preoperative planning of VHD to exclude coronary artery disease (CAD) and in the follow-up of valve replacement. This chapter provides the basis of VHD pathophysiology in the elderly with reference to echocardiographic diagnostic criteria and finally focuses on the most recent clinical applications of MRI and CT in this setting.

12.2 Anatomy of the Cardiac Valves

The heart is a hollow organ divided into four chambers, two atria and two ventricles, coupled into two atrioventricular pumps (right and left heart) independent of each other and separated by interatrial and interventricular septa. The heart is a pump that circulates the blood in the vessels by the pulmonary and systemic circulations. The superior and inferior vena cava lead the systemic venous blood to the right atrium and from here via the tricuspid valve to the right ventricle. Systolic contraction pumps the blood via the pulmonary valve into the pulmonary artery and pulmonary circle. Oxygenated blood is conveyed to the pulmonary veins (usually four, often with variable number and branching), which drain into the left atrium and from here via the mitral valve into the left ventricle. Then, systolic contraction pumps the blood through the aortic valve into the systemic circulation.

Therefore, cardiac valves regulate the unidirectional flow between the cardiac chambers and the great vessels. The tricuspid and mitral valves regulate the atrioventricular flow. The tricuspid is the three-flapped (composed of septal, inferior, and anterosuperior leaflets) valve of the right section of the heart, while the mitral is the two-flapped (composed of aortic and mural leaflets) valve of the left section. The mitral valve area ranges from 4 to 6 cm^2. In the longitudinal cardiac axis, the tricuspid valve is always positioned more cranially to the mitral valve. Chordae tendineae (thickness 0.4–1.2 mm for the mitral valve) connect the leaflets to the papillary muscles of the ventricles, preventing valve prolapse and backflow. The apparatus of the tricuspid incorporates three papillary muscles: anterior (the largest), medial, and inferior. The apparatus of the mitral valve includes two paired papillary muscles incorporated in the anterolateral and posteromedial walls of the left ventricle (Ranganathan et al. 1970).

The pulmonic and aortic valves are called semilunar because of their crescent shape. The pulmonary valve is placed at the junction of the right ventricle and pulmonary artery; the aortic valve is positioned at the junction of the left ventricle and aorta. Both valves lack chordae tendineae. The semilunar valves are made up of three leaflets which open as pressure rises in the ventricles and close as pressure increases in the pulmonary artery and aorta, preventing backflow of blood from the great arteries into the ventricles. The pulmonary artery arises from the

outflow tract of the right ventricle via the pulmonary valve. The infundibular muscles separate the leaflets of the pulmonic and tricuspid valves. The aortic valve presents usually three leaflets with corresponding sinuses, commissures, and coronary artery ostia; the area of the normal aortic valve varies from 2.5 to 4 cm^2 (Brickner et al. 2000). The aortic root connects the aorta to the atrioventricular fibrous annulus and myocardium. The first tract of the aorta is dilated, because of the swellings of the sinuses, and is called the bulb. There are usually three aortic sinuses (known also as the Valsalva sinuses): the right anterior sinus giving rise to the right coronary artery, the left posterior sinus giving rise to the left coronary artery, and the posterior noncoronary sinus. The junction between the aortic root containing the sinuses of Valsalva and the ascending aorta is called the sinotubular junction. The right coronary artery arises from an ostium located in the middle of the right sinus of Valsalva. The left main coronary trunk originates from the middle portion of the left sinus of Valsalva giving rise to the left anterior descending and circumflex arteries. A split origin of the left anterior descending and circumflex arteries from the left sinus of Valsalva may be observed (0.67 %), as well as a large number of coronary origin and course anomalies (Angelini et al. 2002).

The most common congenital valve anomaly is the bicuspid aortic valve which involves 0.5–1 % of the population (Basso et al. 2004) and occurs in 13.7 per 1,000 people (Hoffman and Kaplan 2002). The bicuspid valve is typically made of two unequal-sized cusps instead of three. It is often asymptomatic in childhood and misdiagnosed. However, the abnormal shear stress leads progressively to valve calcification and stenosis, or in some cases to aortic root dilation (Tzemos et al. 2008). Bicuspid aortic valve may be associated with aorta coarctation (Ciotti et al. 2006).

12.3 Valvular Heart Disease

12.3.1 Pathophysiology

Although VHD is less common in developed countries than CAD, heart failure, or hypertension, aging populations and considerable advances in diagnosis and treatment have led to a new interest in the field. The decline of acute rheumatic fever due to better prophylaxis of streptococcus infections highlights the decrease in the incidence of rheumatic valve disease, whereas increased life expectancy accounts for the raise of degenerative VHD in western countries. Nowadays, the most frequent VHD are aortic stenosis (AS) and mitral regurgitation (MR), whereas aortic regurgitation (AR) and mitral stenosis (MS) have become less common. However, rheumatic heart disease is still present in developed countries because of immigration and sequelae of rheumatic fever in elderly patients. The treatment for severe and acute VHD is valve replacement with prosthetic devices by means of conservative surgical approaches or with new percutaneous interventional techniques.

12.3.1.1 Mitral Stenosis

The major cause of MS is rheumatic fever, which affects women more frequently and induces progressive changes of the mitral valve: inflammatory responses, such as thickening at the leaflet edges, fusion of the commissures, and chordal shortening, and scarring features, such as fibrosis, increased collagen and tissue cellularity, and finally calcification (Sagie et al. 1996). The valve may present a "fish mouth" appearance because of the symmetric fusion of the commissures resulting in a small oval orifice in diastole. At end stages the thickened leaflets may be adherent and rigid leading to combined MS and MR. Reduction of mitral valve orifice (<1.5 cm^2 in moderate MS; <1 cm^2 in severe MS) determines an increase in transmitral gradient, and sequentially in the left atrial, pulmonary circle, and right heart pressures. Exertional dyspnea may be precipitated by tachycardia and atrial fibrillation in elderly patients and trigger loop mechanisms of left atrial pressure elevation (Fuster et al. 2006). Left atrial enlargement is associated with an increased risk of thrombus formation and systemic embolism. A number of conditions in the elderly may simulate the pathophysiology of MS: extensive mitral annular calcification, thrombus or myxoma in the left atrium, and large vegetations of infective endocarditis.

12.3.1.2 Mitral Regurgitation

Abnormalities in any component of the mitral valve apparatus may lead to MR. The most common causes of organic MR include mitral valve prolapse, rheumatic heart disease, infective endocarditis, ischemic heart disease (with papillary muscle rupture), and collagen vascular disease. MR may be also functional and secondary to dilation of the left ventricle. MR may be acute in case of chordae tendineae or papillary muscle rupture, or infective endocarditis. Mitral valve prolapse (1–2 % of the population) refers to a systolic billowing of mitral leaflets into the left atrium, which is usually asymptomatic, but may lead to severe MR (Freed et al. 2002). In severe MR, the unprepared left cardiac chambers cannot accommodate the regurgitant volume, which causes pulmonary congestion and edema. In these patients valve repair or replacement must often be performed urgently. Patients with mild to moderate MR may remain asymptomatic for many years; however, MR tends to develop over time with a slightly increase in volume overload due to an enlargement of the effective orifice area (Enriquez-Sarano et al. 1999). Eccentric left ventricle hypertrophy and dilation may consequently compensate the increase in volume overload.

12.3.1.3 Aortic Stenosis

AS has become the most frequent type of VHD in Europe and North America, primarily presenting as degenerative calcific stenosis in the elderly. Defined as an irregular valve thickening without obstruction to left ventricular outflow, AS is present in about 25 % of adults over 65 years. AS is widely associated with cardiovascular risk factors (Stewart et al. 1997) and adverse clinical outcome (Otto et al. 1999). The left ventricle gradually adapts to the systolic pressure overload through concentric hypertrophy. However, if the hypertrophic process is inadequate and relative wall thickness does not increase in proportion to pressure, wall stress increases and the high afterload causes a decrease in ejection fraction (Krayenbuehl et al. 1988). Unfortunately, the hypertrophic heart may have reduced coronary perfusion, even in the absence of CAD (Bache et al. 1981). Then, exercise or tachycardia can produce a misdistribution of coronary blood flow and subendocardial ischemia, which can worsen left ventricular dysfunction. Another issue that is particularly common in elderly patients, especially in women, is the inappropriate degree of hypertrophy associated with high perioperative morbidity and mortality (Aurigemma et al. 1994).

12.3.1.4 Aortic Regurgitation

Etiology of AR includes idiopathic dilation of the aorta, congenital abnormalities (bicuspid valves), calcific degeneration, rheumatic disease, infective endocarditis, systemic hypertension, myxomatous degeneration, dissection of the ascending aorta, and Marfan syndrome. AR may be acute (infective endocarditis, aortic dissection, and trauma) or more often chronic. Dilation of the aortic root determines tension and bowing of the individual cusps, which may thicken, retract, and become too short to close the orifice. AR secondary to marked dilation of the ascending aorta is now more common than primary valve disease in patients undergoing valve replacement (Gelfand et al. 2006). The left ventricle responds to the overload of chronic AR with a series of compensatory mechanisms, including an increase in end-diastolic volume and chamber compliance, and a combination of eccentric and concentric hypertrophy. In a large subset of patients, the balance between afterload excess, preload reserve, and hypertrophy cannot be accommodated indefinitely, so that the reduction of ejection fraction leads to dyspnea, and the diminished coronary flow reserve leads to exertional angina and myocardial ischemia (Nitenberg et al. 1988). In acute severe AR, compensatory mechanisms are not efficient to accommodate the volume overload and patients present with pulmonary edema or cardiogenic shock.

12.3.1.5 Right-Sided Valve Disease

Tricuspid stenosis (TS), which is almost exclusively of rheumatic origin, is rarely observed. It is almost always associated with left-sided valve lesions which dominate the presentation. A relatively modest diastolic pressure gradient (>5 mmHg) is usually sufficient to elevate right

atrial pressure to levels that result in systemic venous congestion. Tricuspid regurgitation (TR) is more often a functional rather than a primary lesion, depending on the annular dilation secondary to right ventricular pressure and/or volume overload associated with pulmonary hypertension and left-sided VHD. TR can also occur secondary to right ventricle infarction (Rivera et al. 1993).

Pulmonary valve stenosis is often congenital, while regurgitation may occur secondary to pulmonary hypertension and dilation of the pulmonary artery in connective tissue disorders.

12.3.2 Echocardiography

Echocardiography still remains the reference standard to evaluate valve structure and function (Figs. 12.1 and 12.2). It has been widely deployed for the assessment of VHD because of its high accessibility and cost-effectiveness (Vahanian et al. 2007; Bonow et al. 2006). The main limitations of echocardiography are operator dependence and poor acoustic window in obese patients.

12.3.2.1 Mitral Stenosis

Transthoracic echocardiography (TTE) is the main method to assess the severity and consequences of MS. Severity of MS should be quantified using two-dimensional planimetry and the pressure half-time method, which are complementary approaches for measuring valve area (Table 12.1) (Bonow et al. 2008). Echocardiography may also evaluate pulmonary artery pressures, the presence of associated MR, and the size of the left atrium.

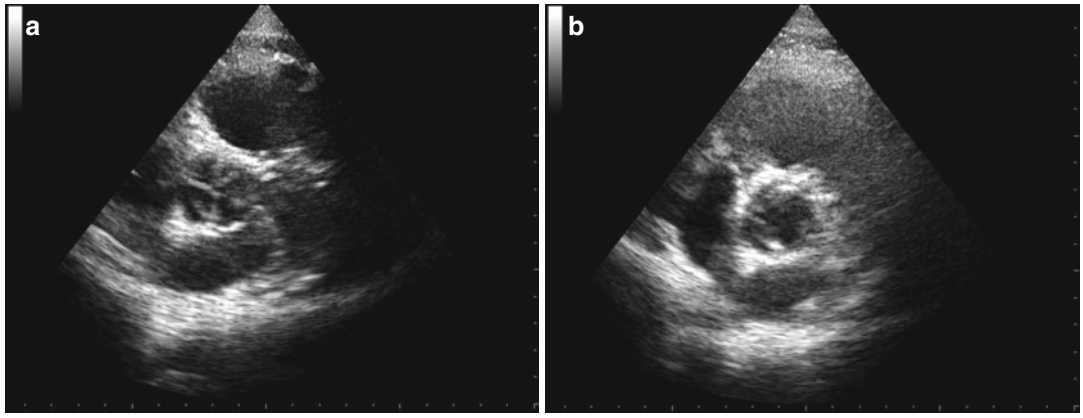

Fig. 12.1 TTE images of aortic valve in diastolic (**a**) and systolic (**b**) phase

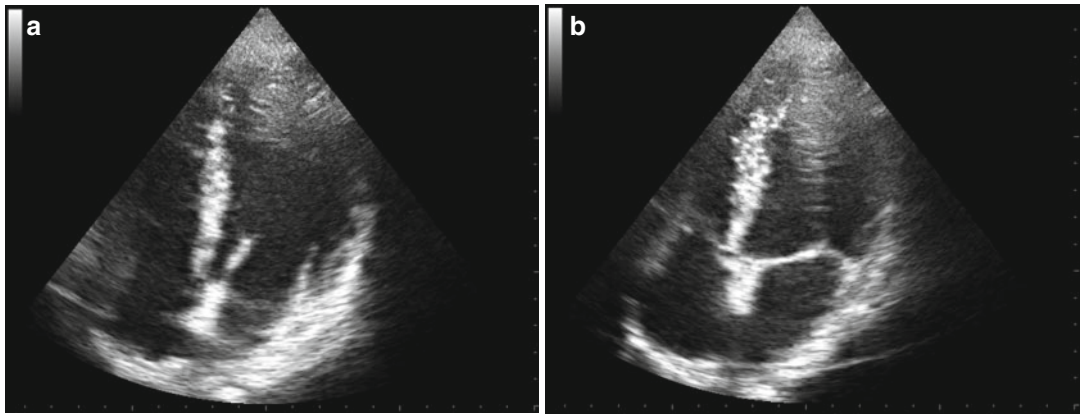

Fig. 12.2 TTE images of mitral valve in diastolic (**a**) and systolic (**b**) phase

Transesophageal examination (TEE) should be performed to exclude left atrial thrombosis before percutaneous mitral commissurotomy, or after an embolic episode, or when TTE provides suboptimal information. Stress tests may be helpful in patients with unclear symptoms.

12.3.2.2 Mitral Regurgitation

Echocardiography is the pivotal examination and must include the assessment of severity and consequences of MR. Several methods can be used to determine the severity of MR (Table 12.2) (Bonow et al. 2008). TTE may reveal a central color flow jet in a structurally normal apparatus suggesting annular dilation from left ventricle dilation or tethering of the posterior leaflet, because of regional dysfunction in patients with ischemic heart disease. TTE may display eccentric flow jet of MR with abnormalities of the valve apparatus (calcifications, thickening, and redundancy of leaflets) indicating organic MR. Color flow mapping of regurgitant jets is the easiest diagnostic method, but its accuracy is limited. Quantitative methods to measure regurgitant fraction, regurgitant volume, and effective regurgitant orifice area are more accurate. In the hemodynamically stable patient, if CAD is suspected, conventional coronary angiography should be performed to plan a potential myocardial revascularization.

Table 12.1 Echocardiographic criteria of mitral stenosis severity

Features	Mild	Moderate	Severe
Mean gradient (mmHg)	<5	5–10	>10
Pulmonary artery systolic pressure (mmHg)	<30	30–50	>50
Valve area (cm^2)	>1.5	1.0–1.5	<1.0

12.3.2.3 Aortic Stenosis

TTE is useful for evaluation of aortic valve anatomy and function and for determining the left ventricle response to pressure overload. Severity of AS can be easily defined with Doppler echocardiographic measurements of aortic jet velocity, mean transvalvular pressure gradient, and valve area (Table 12.3) (Cheitlin et al. 2003; Bonow et al. 2008). Stress echocardiography using low-dose dobutamine may be helpful to distinguish truly severe AS from the rare case of pseudo-severe AS, in which patients present a functional small valve area. Severe AS shows only small changes in valve area (<0.2 cm^2) with increasing flow rate but significant increase in gradients (>50 mmHg). TEE is needed when valve planimetry of TTE is inadequate.

12.3.2.4 Aortic Regurgitation

Echocardiography may identify the cause of AR by demonstrating bicuspid valve, thickening of the cusps, prolapse, flail leaflet, or vegetations. TTE is useful for the measurement of left ventricle end-diastolic and end-systolic dimensions and volumes, ejection fraction, and mass. In addition, the size and shape of the aortic root can be evaluated, although visualization of the ascending aorta is not always adequate and may require additional imaging procedures such as TEE, CT, or MRI. Doppler echocardiography and color flow Doppler imaging are the most accurate techniques in the evaluation of AR (Table 12.4) (Bonow et al. 2008).

Table 12.2 Echocardiographic criteria of mitral regurgitation severity

Features	Mild	Moderate	Severe
Color Doppler jet area	<4 cm^2	Greater than mild	>40 % of LA
	<20 % LA area	No criteria for severe MR	Swirling in LA
Doppler vena contracta width (cm)	<0.3	0.3–0.69	≥ 0.70
Regurgitant volume (ml/beat)	<30	30–59	≥60
Regurgitant fraction (%)	<30	30–49	≥50
Regurgitant orifice area (cm^2)	<0.20	0.2–0.39	≥0.40
Left atrial size			Enlarged
Left ventricular size			Enlarged

LA left atrial, *MR* mitral regurgitation

12.3.2.5 Right-Sided Valve Disease

TTE may assess tricuspid valve structure and motion (severe TS: valve area <1 cm^2). Doppler echocardiography permits estimation of the severity of TR (severe TR: vena contracta width >0.7 cm, systolic backflow in hepatic veins) (Bonow et al. 2008). TTE may also show abnormal motion of the septum which is characteristic of right ventricle volume overload in diastole and/or septal flutter. Abnormal Doppler signals in the right ventricle outflow tract are observed in patients with severe pulmonic stenosis (jet velocity >4 m/s; gradient >60 mmHg) or with pulmonic regurgitation secondary to pulmonary hypertension (color jet; continuous signal with a sharp deceleration slope) (Bonow et al. 2008).

12.4 Magnetic Resonance Imaging

12.4.1 Technique

Doppler echocardiography with color flow mapping has considerably affected the diagnostic work-up for the evaluation of VHD. However, TTE may not be conclusive in patients with poor acoustic windows; it is operator dependent and relies on several geometric assumptions particularly for the quantification of regurgitant lesions and the measurement of left ventricular systolic function. Invasive techniques such as cardiac catheterization may be employed in the preoperative evaluation of the coronary arteries, quantification of cardiac hemodynamic, or investigation of discrepancies between symptoms and echocardiography data. Several papers have demonstrated that MRI may be a promising alternative or complement to TTE (Globits and Higgins 1995). Noninvasive MRI supplies three-dimensional anatomy and functional assessment, with a potentially more accurate measurement of ventricular function than echocardiography (Higgins and Sakuma 1996).

The most widely used cine pulse sequence on MRI to assess valve anatomy and ventricle function is the balanced steady-state free precession (b-SSFP) sequence (Fig. 12.3). High contrast between blood pool and surrounding structures is achieved with excellent spatial (in-plane resolution of 1.4 mm) and temporal resolution (~35 ms). SSFP sequences have several monikers, such as TrueFISP (Siemens), balanced FFE (Philips), and FIESTA (General Electric) (Karamitsos and Myerson 2011). All fast gradient echo (GE) sequences are SSFP. b-SSFP is a special type of SSFP sequence in which the gradient-induced dephasing within repetition time is exactly zero. Within repetition time each applied gradient pulse is compensated by a pulse with opposite polarity, which ensures the complete recovery of transverse magnetization. While the classic spin-echo sequence shows either a T1- or a T2-weighted (T1w or T2w) contrast, b-SSFP combines T1 and T2 contributions (Bogaert et al. 2005). b-SSFP requires a short repetition time (3–6 ms) to minimize artifacts and relatively

Table 12.3 Echocardiographic criteria of aortic stenosis severity

Features	Mild	Moderate	Severe
Jet velocity (m/s)	<3.0	3.0–4.0	>4.0
Mean gradient (mmHg)	<25	25–40	>40
Valve area (cm^2)	>1.5	1.0–1.5	<1.0
Valve area index (cm^2/m^2)			<0.6

Table 12.4 Echocardiographic criteria of aortic regurgitation severity

Features	Mild	Moderate	Severe
Color Doppler jet width	<25 % of LVOT	Greater than mild; no criteria for severe AR	>65 % of LVOT
Doppler vena contracta width (cm)	<0.3	0.3–0.6	>0.6
Regurgitant volume (ml/beat)	<30	30–59	≥60
Regurgitant fraction (%)	<30	30–49	≥50
Regurgitant orifice area (cm^2)	<0.10	0.10–0.29	≥0.30
Left ventricular size			Increased

LVOT left ventricular outflow tract, *AR* aortic regurgitation

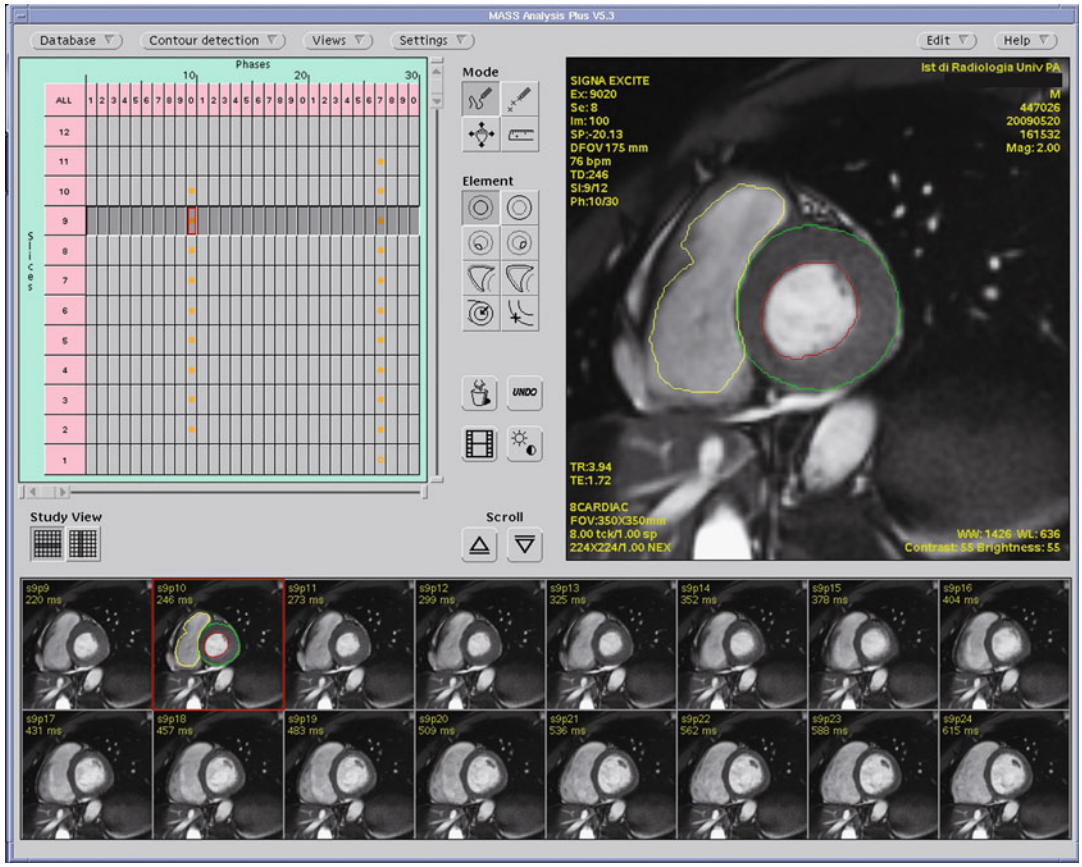

Fig. 12.3 Post-processing software for detection of endocardial and epicardial borders and assessment of functional parameters with b-SSFP images

broad flip angles (between 50° and 80°) to generate the highest signal. Images are acquired with RR interval electrocardiography-synchronization. Thirty frames are usually sufficient to evaluate the entire cardiac cycle in a cine loop, allowing a dynamic approach.

Phase contrast (PC) sequences employ the phenomenon of phase shift. PC sequences allow assessment of the blood flow qualitatively and quantitatively in the arterial and venous circle providing information on volume, speed, and direction of flow. Both stationary spins and moving spins along the direction of field gradient undergo phase variations. The variations in the spins that constitute stationary tissue depend on their spatial position and always keep the same intensity with a linear function. On the other side the moving spins act differently since the phase variation induced by the field gradient in one direction depends on the position as well as on the speed and direction of flow which varies proportionally with time (Lombardi and Bartolozzi 2004). A bipolar gradient (first positive, then negative) with equal but opposite amplitude is applied to the GE sequence. Due to the bipolar pulse, flowing spins acquire a phase angle that is, in a first approach, proportional to the amplitude of the gradients and the velocity of the spins. The velocity of the spins can thus be measured from the phase angle. The bipolar gradient is applied independently in each direction (x, y, z) of the magnetic field and presents an amplitude proportional to the flow the operator requires (VENC, velocity encoding value). Stationary field inhomogeneities due to high magnetic susceptibility may be avoided by acquiring two identical sequences that differ only in the activation of the bipolar gradient; the two data sets are subtracted,

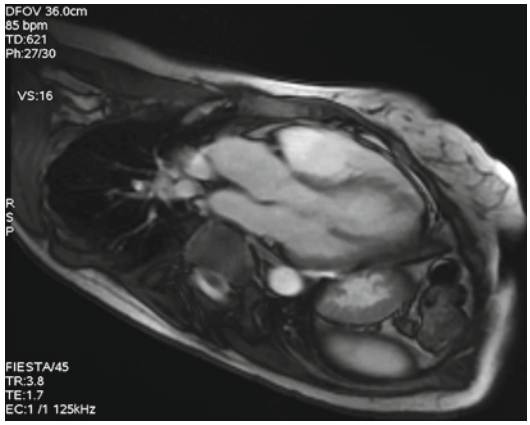

Fig. 12.4 b-SSFP three-chamber view of the heart to plan phase contrast sequence

removing the signal of the stationary tissue. The signal related exclusively to the blood flow is maintained (Figs. 12.4 and 12.5).

Currently, the morphologic fast spin-echo (FSE), turbo spin-echo (TSE), or black-blood T1w or T2w sequences are not the first choice for evaluation of patients with VHD but sometimes may provide valuable additional information. Visualization of myocardial edema is optimal with T2w acquisition, whereas other indications such as ventricular wall thickness and pericardial thickening benefit from T1w acquisition. The visualization of enhancing structures (infarction, mass, fibrosis) after intravenous injection of contrast agents also needs a T1w approach. In T1w

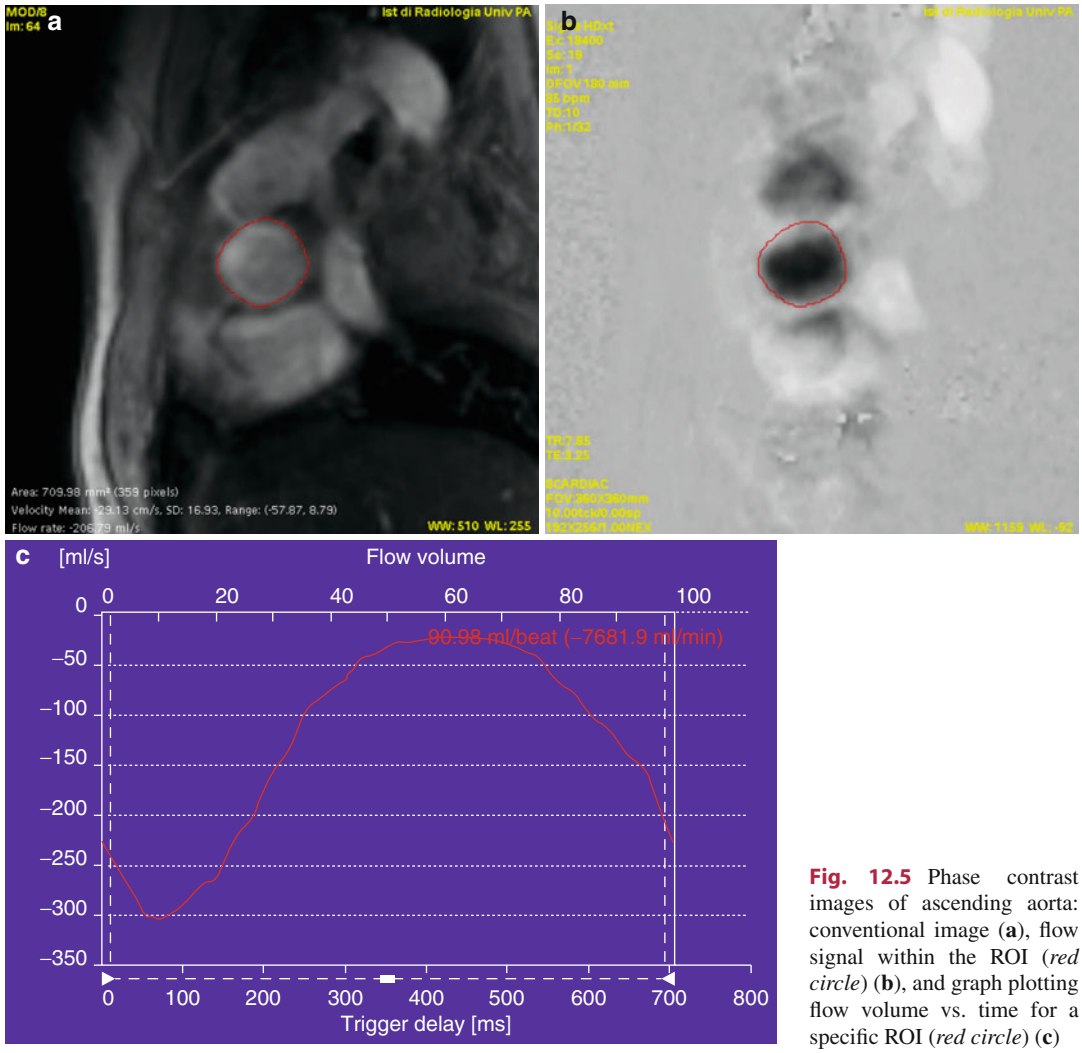

Fig. 12.5 Phase contrast images of ascending aorta: conventional image (**a**), flow signal within the ROI (*red circle*) (**b**), and graph plotting flow volume vs. time for a specific ROI (*red circle*) (**c**)

the echo time (TE) is kept short (5–15 ms) and repetition time is chosen to overlap with one single RR interval of the ECG. Images are acquired by obtaining a number of k-space lines (typically 9–15) every diastole to reduce motion artifacts. T2w acquisitions can be performed with faster protocols. In T2w TSE the turbo factor is usually higher (21–33) and the repetition time is longer (two or three heartbeats), which is advantageous for T2w contrast acquisitions. Furthermore, image contrast may be increased by fat-suppression techniques or by black-blood pulse (Bogaert et al. 2005).

Coexisting myocardial infarction, even unknown, is not an atypical finding in patients with VHD. Patterns of focal fibrosis (nonischemic cardiomyopathy) or scarring due to prior myocardial infarction can be identified with the late gadolinium enhancement technique which employs an inversion recovery gradient echo (IR-GE) with an initial 180° inversion pulse greatly increasing the T1w of images. The acquisition is performed in diastole, whereby it is necessary to define carefully the inversion time (TI), labeled as the time between the application of the 180° prepulse and the center of k-space (Simonetti et al. 2001). In this phase the magnetization of the normal myocardium is close to zero. Hence, the viable myocardium is hypointense, while the necrotic myocardium appears clearly hyperintense. If the acquisition sequence is properly optimized (TI ranges from 150 to 600 ms at 1.5T), the signal intensity of the necrotic area is >500 % compared to baseline and a clear distinction between necrotic and viable tissue is depicted (Fieno et al. 2000).

12.4.2 Applications

Cardiac magnetic resonance (CMR) is considered a second-level technique with respect to echocardiography; however, it may be extremely useful in selected patients with MS. CMR provides optimal visualization of the restricted mitral leaflets, particularly on the left ventricular outflow tract view. Elevation of left atrial outflow resistance occurs when the mitral valve area is below 2 cm^2. This leads to an increase in the diastolic transmitral gradient, which can be assessed by measuring the peak velocity across the mitral valve. Peak velocity measurements across the mitral valve with short-axis view below the valvular plane correlate well with Doppler measurements at TTE (Heidenreich et al. 1995). However, plane positioning must be accurate to obtain precise measurements of the valve area. Diastolic flow and velocity can also be measured in this plane, and pressure half-time calculated as for TTE (Lin et al. 2004), although associated atrial fibrillation in severe MS decreases the accuracy of flow measurements (Myerson et al. 2010). In severe MS the pulmonary vein flow is inverted. The consequences of MS such as left atrial enlargement, pulmonary edema, right ventricular dysfunction, and pulmonary valve regurgitation may be comprehensively evaluated. Moreover, the presence of atrial thrombus secondary to fibrillation should be assessed in all patients.

CMR can evaluate mitral leaflet morphology and establish the cause of MR with good agreement to TEE. Multislice contiguous cine acquisition of 5-mm thickness may be employed for a comprehensive assessment of morphology and detection of prolapse/regurgitation (Chan et al. 2008). The qualitative assessment of the severity of MR can be obtained by visualization of the signal void of the regurgitant jet on cine SSFP sequences (Fig. 12.6). A narrow jet suggests lower degrees of regurgitation, while a wide jet with a core of high signal indicates a more severe regurgitation. Quantification of MR is usually performed indirectly by subtracting aortic systolic flow (measured by aortic flow mapping) from left ventricular stroke volume (Kramer et al. 2008). Direct quantification of MR is possible using through-plane flow mapping on the atrial side of the mitral valve, although it is problematic due to the rapidly moving valve and often eccentric jets of regurgitation. A combination of SSFP and PC is often used to obtain indirect quantification of MR with reproducible agreement with echocardiography and angiography, predicting the future need for surgery in asymptomatic patients (Kon et al. 2004). The mitral orifice may be measured on images parallel to the

annulus in systole, nonetheless with less accuracy in coexisting leaflet calcifications. CMR may detect ultimate hemodynamic consequences of MR such as left ventricle dilation and failure.

The excellent visualization of anatomy provided by SSFP cines allows accurate evaluation of the severity of AS with direct planimetry of the orifice. A good agreement in valve area planimetry was found between CMR with SSFP cines and TEE (John et al. 2003). Continuity equations can also be used to estimate the valve area with direct measurement of the left ventricle outflow tract area (Figs. 12.7 and 12.8) (Garcia et al. 2011). Measurement of velocity is beneficial in distorted aortic roots, whereas ultrasound beam alignment with the stenotic jet may be difficult. Furthermore, stenotic jets are often not parallel to the outflow tract and are incorrectly assessed with TTE. Other benefits of CMR include the ability to distinguish subvalvular from supravalvular AS (cine images) and the ability to identify the site of velocity acceleration (in-plane velocity mapping) (Fig. 12.9). CMR may also quantify the increase of left ventricular mass and display the dilation of the aortic root in patients with bicuspid valve (Alegret et al. 2003). The reduction of left ventricular mass after aortic valve replacement may be documented by CMR (Sandstede et al. 2000). Late gadolinium enhancement provides useful information in patients with severe AS since a typical patchy midwall enhancement appears in up to a third of patients, usually associated with ventricle hypertrophy (Debl et al. 2006).

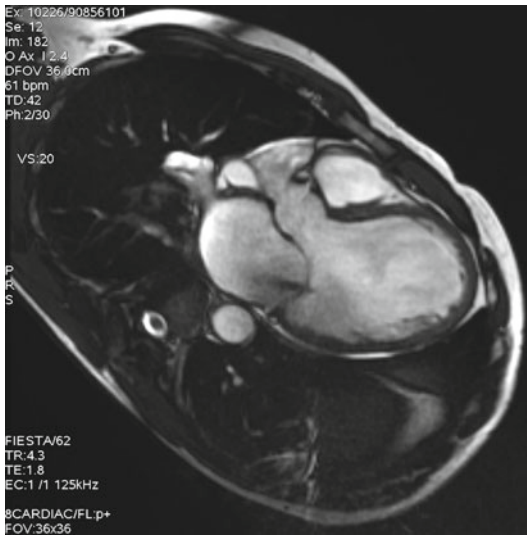

Fig. 12.6 b-SSFP three-chamber view depicting a retrograde central signal void of a regurgitant mitral valve in a patient with post-ischemic dilative cardiomyopathy

CMR provides a direct quantitative assessment of the degree of AR regurgitation (AR volume measured in ml/beat) and its consequences

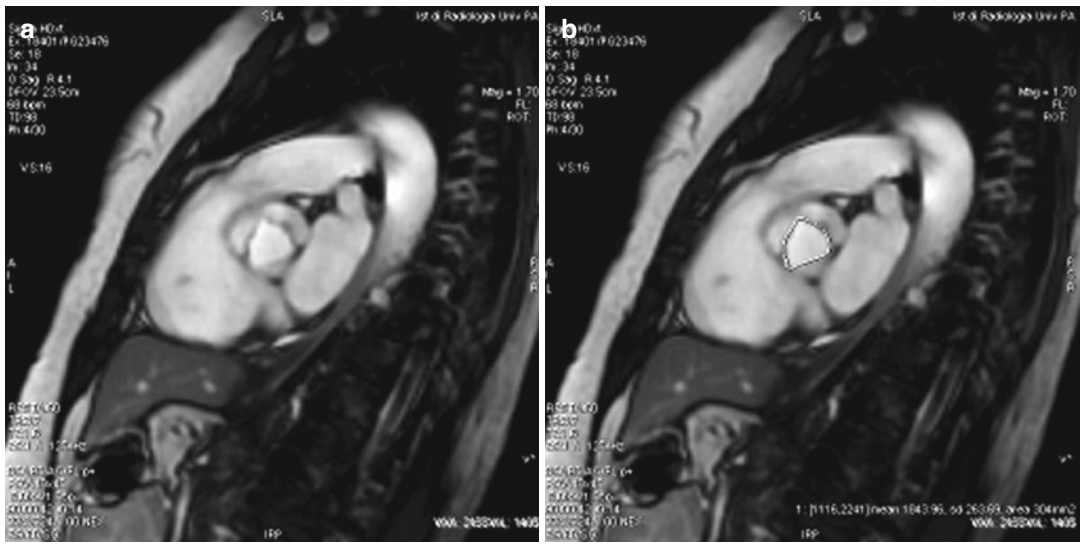

Fig. 12.7 b-SSFP images of aortic valve: qualitative assessment of valve leaflets motion (**a**), measurement of valve area (**b**)

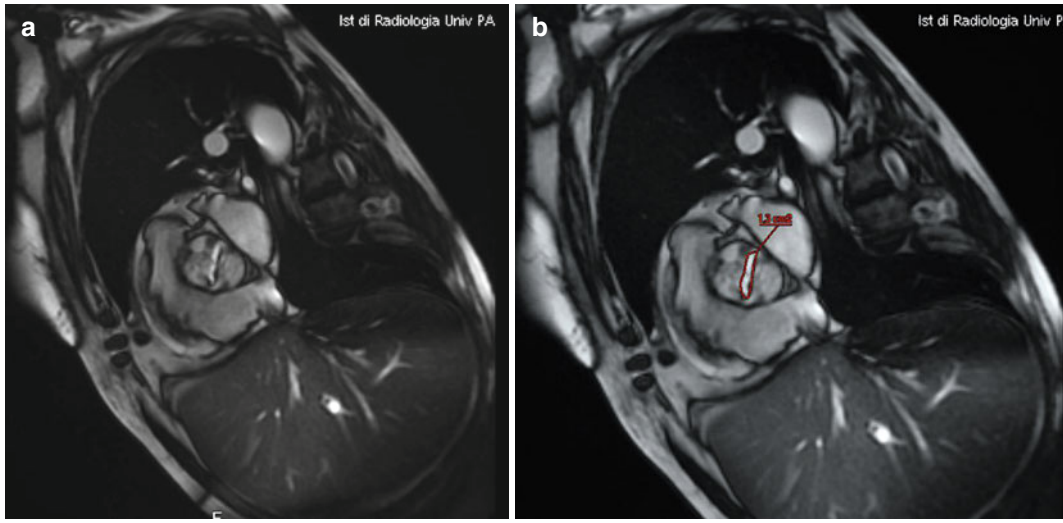

Fig. 12.8 b-SSFP images of stenotic aortic valve: qualitative assessment of aortic valve leaflets motion (**a**), measurement of aortic valve area (**b**)

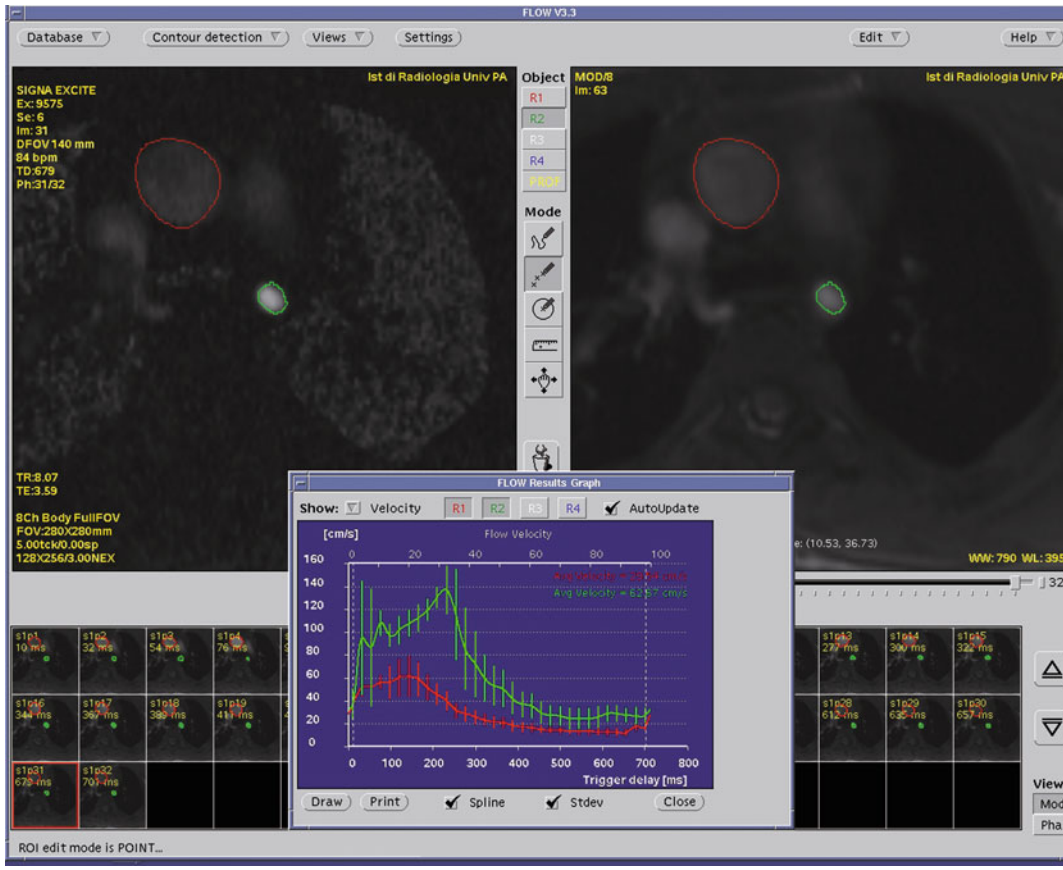

Fig. 12.9 Flow analysis of aortic stenosis with graph of velocity mapping on phase contrast images

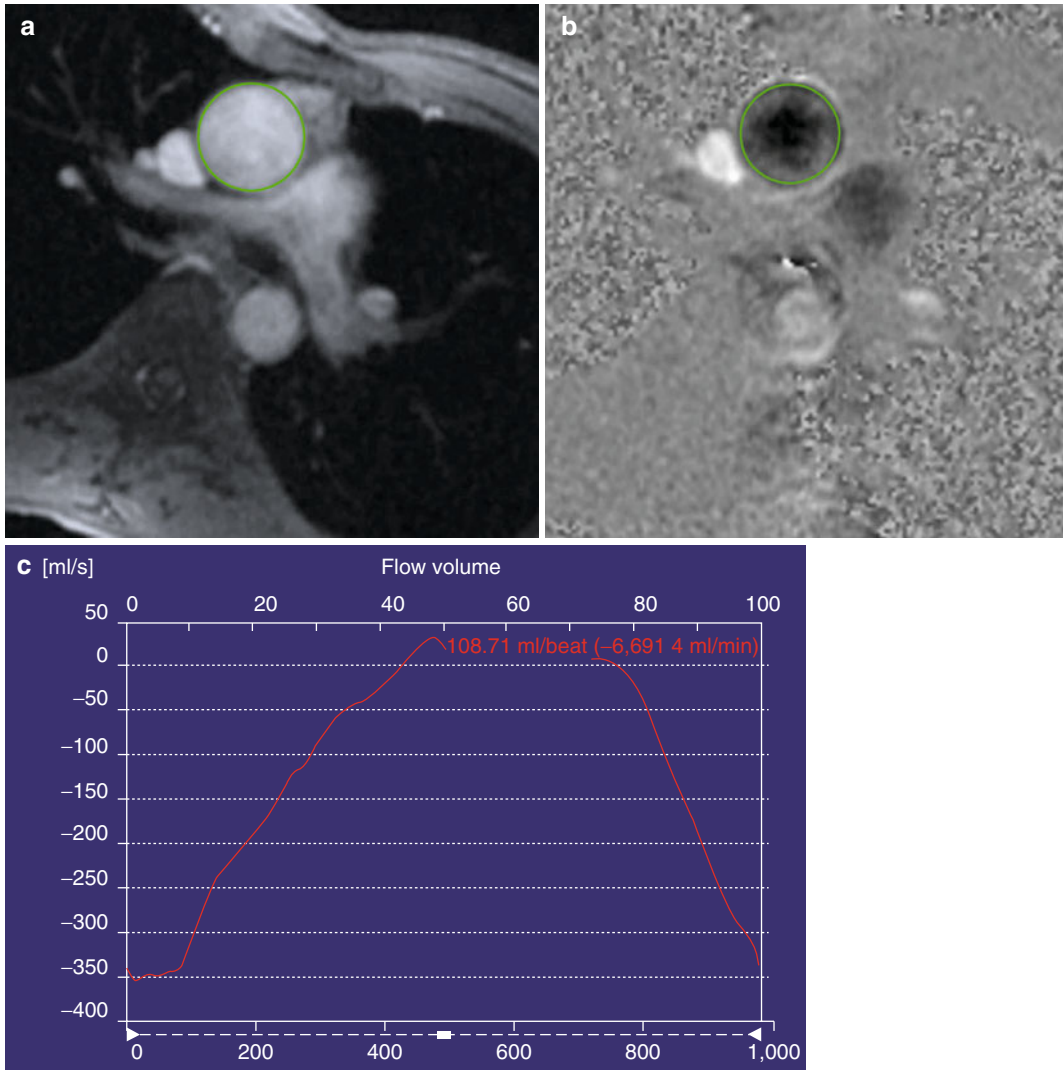

Fig. 12.10 Flow analysis of aortic regurgitation: conventional phase contrast image (**a**), flow map ROI (*green circle*) (**b**), graph plotting view with quantification of aortic regurgitation over the baseline ROI (*green circle*) (**c**)

on left ventricle volumes and function. PC VENC sequences in the slice direction can quantify the regurgitant fraction within an oblique axial plane above the valve (Fig. 12.10). The oblique plane is perpendicular to two orthogonal planes through the ascending aorta, to keep a correct through-plane for the velocity vectors. Positioning of the plane across the aorta is still controversial. In vivo experience suggests that a position between the coronary ostia and the aortic valve may be more accurate than above the coronary ostia (Chatzimavroudis et al. 1997). An alternative approach to quantify AR by CMR is to compare left and right ventricle stroke volumes with cine images. A less accurate assessment of AR can be performed by measuring the signal void of the regurgitant jet on cine imaging (Fig. 12.11). A large jet with an elevated void signal from laminar flow indicates a more severe AR.

Although extremely rare, TS may be assessed with CMR with a direct planimetry of the valve area performed on an image slice through the valve plane in diastole, similarly to MS. CMR may assess TR with SSFP cine sequences

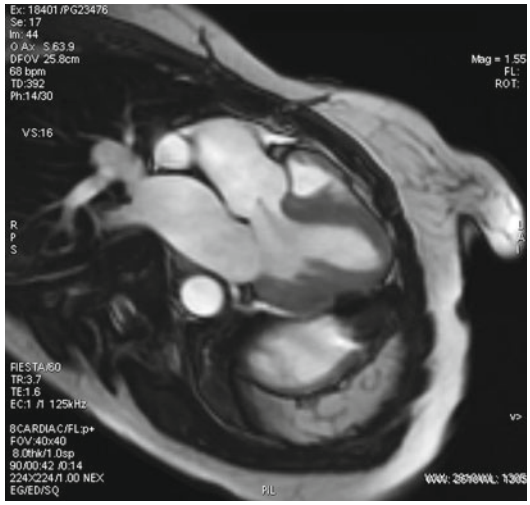

Fig. 12.11 b-SSFP three-chamber view for qualitative assessment of aortic regurgitation with signal void

similarly to MR. The TR jet is evaluated through in-plane velocity mapping in a long-axis right ventricular view. Wider jets (>7 mm) suggest a more severe TR. The calculation of regurgitant volume and fraction is similar to MR. The forward stroke volume, measured in the pulmonary artery with PC acquisition, is subtracted from the total right ventricular stroke volume, acquired with SSFP sequences (Mahle et al. 2003).

Pulmonary regurgitation may be assessed by CMR similarly to AR, although the lower turbulence on cine SSFP images may not allow good visualization. Therefore, in-plane VENC sequences placed just above the pulmonary valve are used to display the regurgitant jet (severe >40 %).

12.5 Computed Tomography

12.5.1 Technique

Computed tomography coronary angiography (CTCA) has been recognized as one of the major innovations in diagnostic imaging over the last decade. CTCA is used to rule out CAD because of its high sensitivity and negative predictive value (Taylor et al. 2010). Furthermore, advances in retrospective ECG-gated CTCA allow morphological and functional evaluation of the cardiac valves. Assessment of valves requires high spatial and temporal resolution to depict small anatomical structures and to minimize cardiac motion artifacts. State of the art 64-slice CT provides a temporal resolution of approximately 165–210 ms, whereas recently introduced scanners can supply an even lower temporal resolution. Compared to echocardiography and CMR, CT provides faster acquisition time and higher spatial resolution, but lower temporal resolution (Chung et al. 2008).

The protocol is basically set up for coronary artery evaluation. However, CT assessment of cardiac valves should optimize image acquisition and reconstruction parameters, as well as the post-processing techniques. Prior to image acquisition oral or intravenous β-blockers may be cautiously administered to lower the heart rate to less than 65 bpm and improve image quality, apart from patients with acute presentation or known severe AS (Mahabadi et al. 2010; Vahanian et al. 2007). The patient is scanned in the craniocaudal direction. Scan fields of view are dependent on the desired clinical information (i.e., preoperative evaluation of valves and coronary artery vs. full thoracic aorta assessment). A breath-hold retrospective ECG-gated acquisition is employed to obtain both static and cine images, with low pitch values and technical parameters between 120 and 140 kV and 350 and 400 mAs.

Rapid intravenous injection of iodinated contrast material (5 ml/s) with bolus tracking is often used. The region of interest is placed within the aortic root, synchronizing the start of the scan with the first arterial passage. The contrast bolus is usually chased with a saline flush. The conventional CTCA protocol aims at a pure arterial visualization of coronary artery tree, aorta, and left chambers, but may produce a heterogeneous enhancement of the right side of the heart. For specific indications (i.e., assessment of right chambers and valves), a lower injection rate or a triphasic protocol (i.e., high-flow infusion of contrast material followed by slower infusion of contrast material and a saline flush) may be employed (Abbara et al. 2009).

Radiation-saving strategies such as prospective ECG gating cannot be used because valve

assessment must be performed throughout the entire cardiac cycle. Retrospective ECG-gated images are reconstructed sequentially at every 5–10 % phase of the RR interval. Dose modulation approaches may be carefully used to lower the dose for a portion of the cardiac cycle depending on the desired cardiac phase (systolic or diastolic) to assess cardiac valves (Chen et al. 2009).

Post-processing of the data set is performed on dedicated workstations and consists of software applications allowing both static and cine images. Multiplanar reconstructions (MPR), maximum intensity projection (MIP), volume rendering (VR), and virtual endoscopy are employed. MPR are reconstructed according to the reference echocardiographic views (four-chamber long-axis, two-chamber long-axis, and two-chamber short-axis views) and allow the cross-section evaluation of valves along the correct planes. Cine images are similarly obtained by combining 10–20 cardiac phases to evaluate opening and closing of valves and ventricular function (Raman et al. 2006).

12.5.2 Applications

CTCA is considered a valuable and appropriate tool in a wide range of heart diseases and has demonstrated its usefulness also in VHD. In particular, CTCA has emerged as a relevant noninvasive imaging technique to exclude CAD (Taylor et al. 2010). In the context of VHD, CT allows morphologic evaluation of the cardiac valves (Figs. 12.12, 12.13, 12.14, 12.15, and 12.16) by visualizing the number and thickness of valve

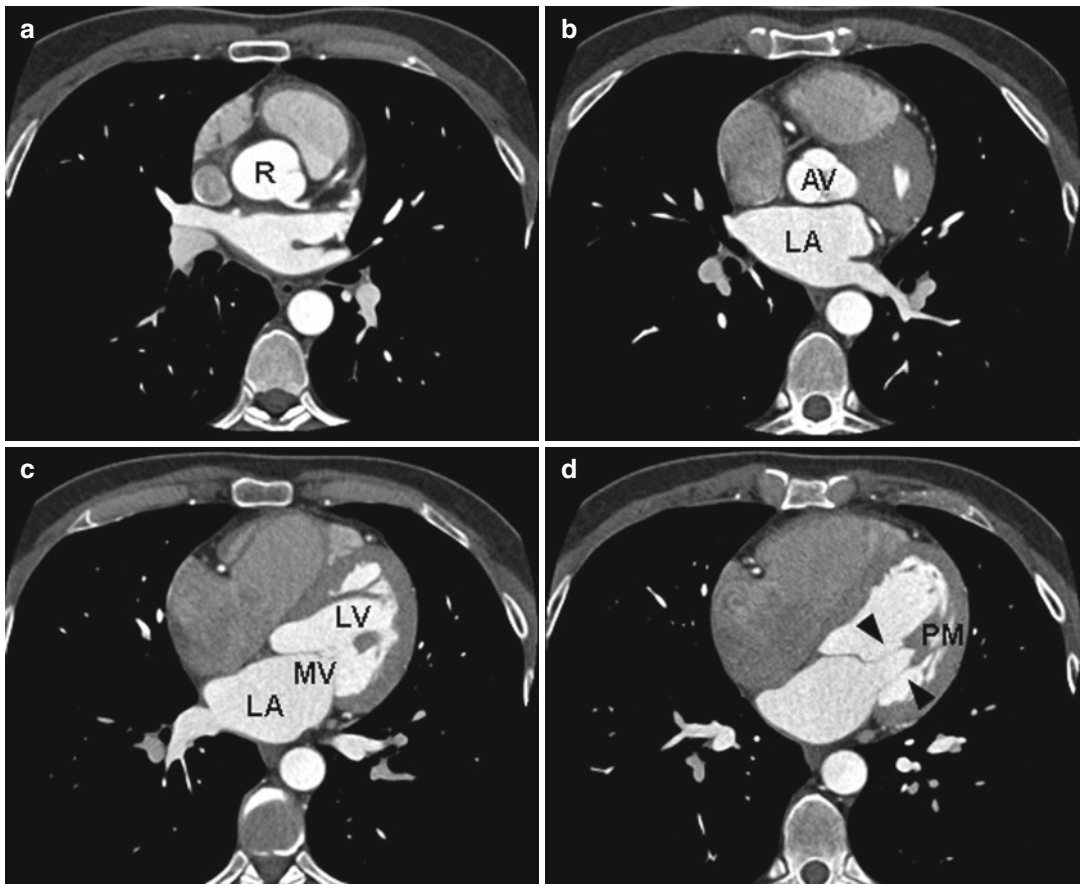

Fig. 12.12 Axial CT views (**a**–**d**) depicting cardiac valves. Aortic root (*R*), aortic valve (*AV*), left atrium (*LA*), mitral valve (*MV*), left ventricle (*LV*), papillary muscles (*PM*), chordae tendineae (*black head arrows*)

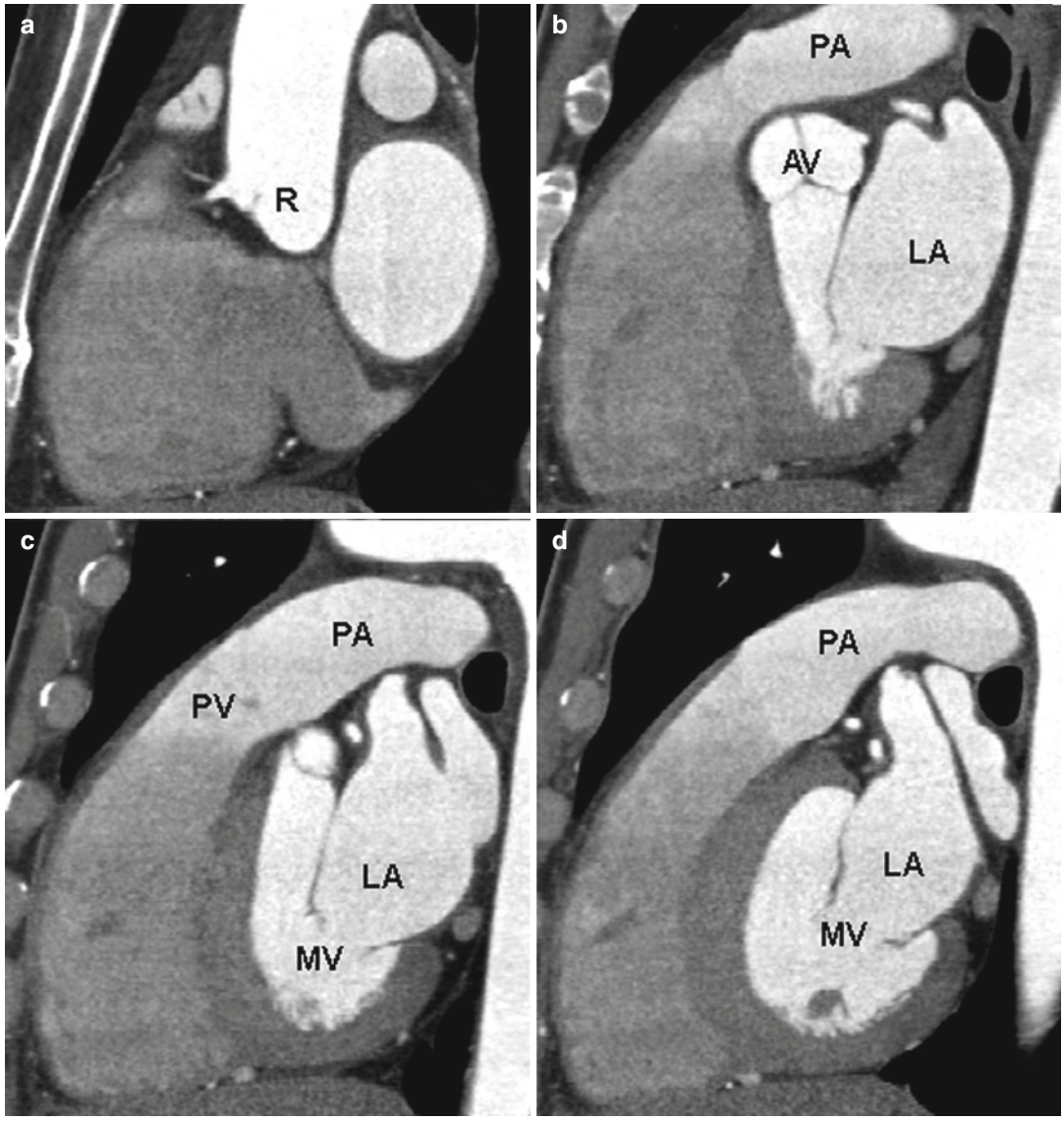

Fig. 12.13 Sagittal CT views (**a**–**d**) depicting cardiac valves. Aortic root (*R*), aortic valve (*AV*), pulmonary artery (*PA*), left atrium (*LA*), pulmonary valve (*PV*), mitral valve (*MV*)

leaflets (i.e., bicuspid vs. tricuspid aortic valve) as well as the presence of calcifications (Willmann et al. 2002). CT may allow a functional assessment of the valves in the setting of congenital and acquired disorders (stenosis and regurgitation).

AS can be evaluated by assessing the thickening and calcification of the cusps and their number (i.e., bicuspid valve) (Fig. 12.17) and excursion (Gilkeson et al. 2006), as well as measuring the area of the valve, which correlates with TEE (Feuchtner et al. 2006a). Aortic valve calcification is associated with the severity of AS (Koos et al. 2006) and presents an annual progression rate of 1.7 %, which increases significantly with age (Owens et al. 2010). Best image quality for aortic valve planimetry is obtained during midsystole to minimize motion artifacts (Abbara et al. 2007). Patients with AS become symptomatic when the aortic valve area reduces to approximately 1 cm^2. The subsequent

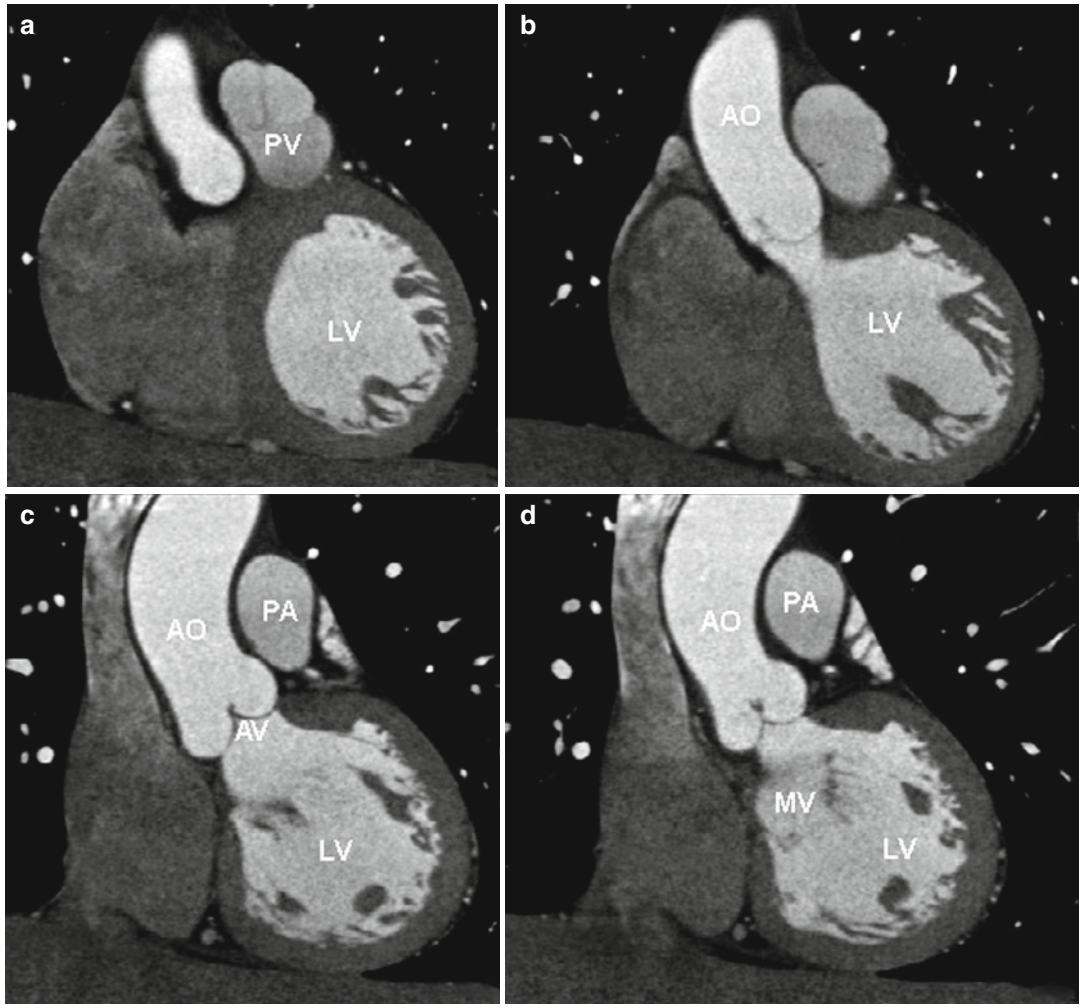

Fig. 12.14 Coronal CT views (**a**–**d**) depicting cardiac valves. Pulmonary valve (*PV*), left ventricle (*LV*), aorta (*AO*), aortic valve (*AV*), pulmonary artery (*PA*), mitral valve (*MV*)

increase of the transvalvular pressure gradient causes the associated dilatation of the ascending aorta, while left ventricular afterload rise leads to concentric ventricular hypertrophy. Both indirect signs of AS may be depicted by CT. CT may also visualize the main findings of AR such as cusp malcoaptation during mid-to-end diastole and central leakage area, with excellent diagnostic accuracy compared to TEE (Feuchtner et al. 2006b). Furthermore, the dilation of the aortic root and the ventricular enlargement may be displayed (Fig. 12.18).

Mitral valve findings (fibrosis, thickening, calcification of leaflets; left chamber enlargement; pulmonary edema and congestion) may be better evaluated in the two-chamber long-axis plane during opening of middiastole. The correlation between CT and TEE is excellent for MS (Messika-Zeitoun et al. 2006). A common complication of MS in the elderly is atrial fibrillation, which may adversely affect ECG-gated CT due to motion artifacts (Sato et al. 2005). Ischemic heart disease due to papillary muscle dysfunction or rupture and post-ischemic dilated cardiomyopathy are considered common causes of functional acute or chronic mitral MR in the elderly (Hickey et al. 1985). CTCA may be helpful in this clinical scenario (Fig. 12.19) (Taylor et al. 2010).

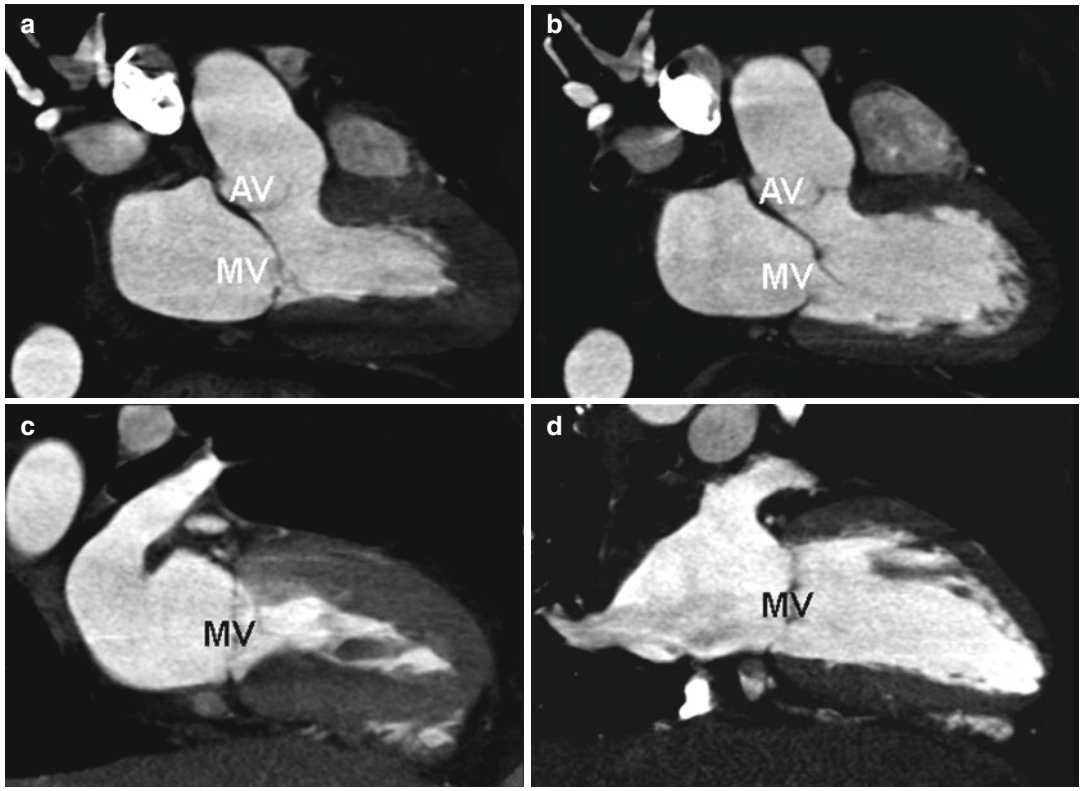

Fig. 12.15 MPR images in aortic and mitral valve planes of the heart during systole (**a**) and diastole (**b**); MPR images long-axis views of the left ventricle during systole (**c**) and diastole (**d**). Aortic valve (*AV*), mitral valve (*MV*)

The right-side valves may be assessed with specific protocols. Indirect signs of right-side overload (dilation of the right chambers, regurgitation of suprahepatic veins, and dilation of the vena cava) may be depicted by CT.

A relevant limitation of CT in VHD assessment is that a retrospective ECG-gated protocol is needed, which requires higher exposure to radiation than the increasingly widespread prospective protocol. Therefore, CT is not primarily used because information from other imaging techniques (echocardiography and MRI) is usually adequate. Furthermore, CT cannot provide a direct measurement of the transvalvular pressure gradient. CT should be performed only in selected patients when the TTE acoustic window is inadequate, when TEE or catheterization are not tolerated, or when MRI is contraindicated (i.e., patients with pacemakers). However, it is reasonable to expect an increasing role for CTCA in the evaluation of cardiac valves because of the technological advances and related dose-reduction strategies.

Candidates for valve replacement may benefit from preoperative CTCA, which can rule out significant CAD (Fig. 12.17) (Meijboom et al. 2006). In addition, CTCA provides the angle of orientation of coronary arteries (normally 120–150°). In patients with bicuspid aortic valves, coronary arteries may have an orientation of 180°. In the event of surgical replacement, it is important to be aware of this condition

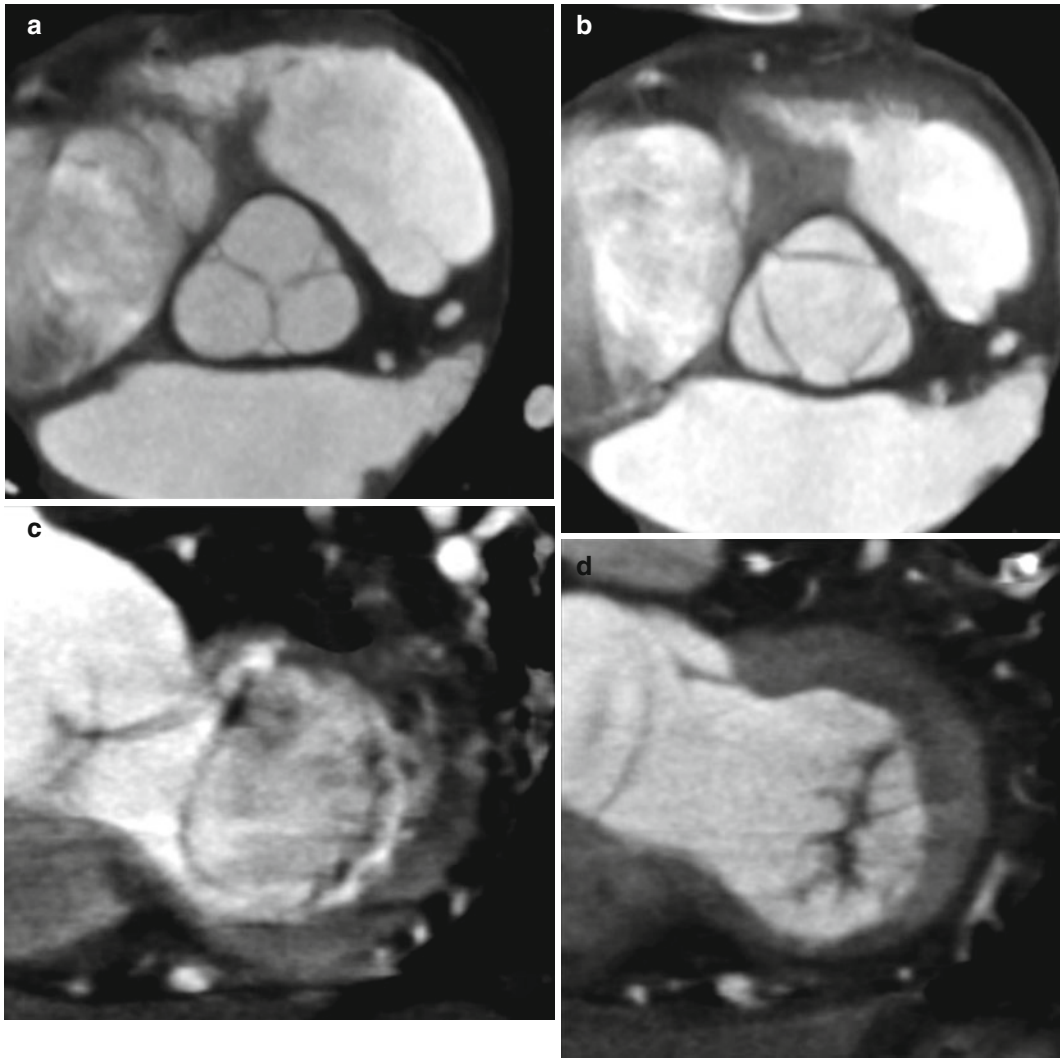

Fig. 12.16 MPR images depict the aortic valve, closed during diastole (**a**) and open during systole (**b**); MPR images display the mitral valve, open during diastole (**c**) and closed during systole (**d**)

(Cademartiri et al. 2007). Coronary anomalies of origin and course may be clearly displayed by CTCA (Cademartiri et al. 2008).

Similarly, postoperative patients with prosthetic valves may benefit from CTCA to assess function and complications, if echocardiography and MRI are inadequate. The progress in CT scanners has improved image quality of valve replacement with considerably decreased artifacts (Habets et al. 2011). Prosthetic complications include thrombus, valve dehiscence, pseudoaneurysm, infective endocarditis, or paravalvular abscess and leaks (Fig. 12.20) (Manghat et al. 2008).

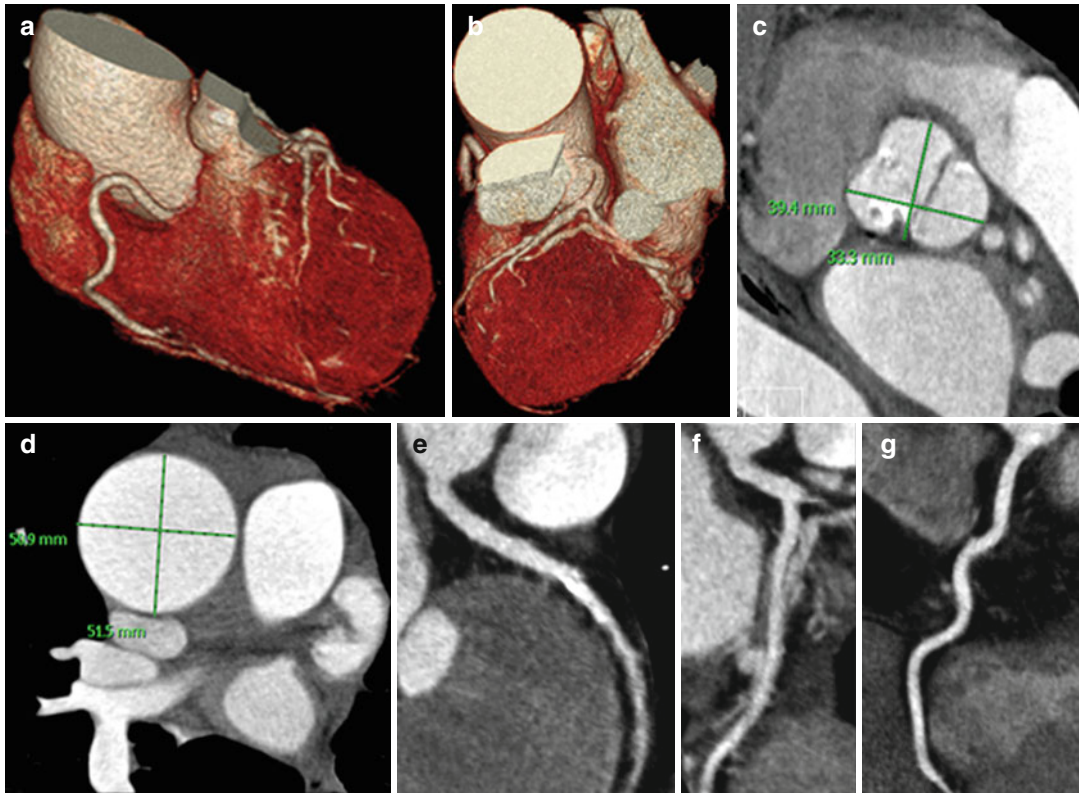

Fig. 12.17 A 63-year-old woman with severe aortic stenosis. VR images display ascending aorta dilation (**a**, **b**); a calcific stenosis of bicuspid valve is depicted by MPR (**c**); accurate measurement of the aneurysm in the cross-sectional view (**d**); MPR images exclude significant coronary artery disease in the right coronary artery (**e**), left anterior descending artery (a calcified nonsignificant plaque is depicted in the midtract (**f**), and circumflex artery (**g**)

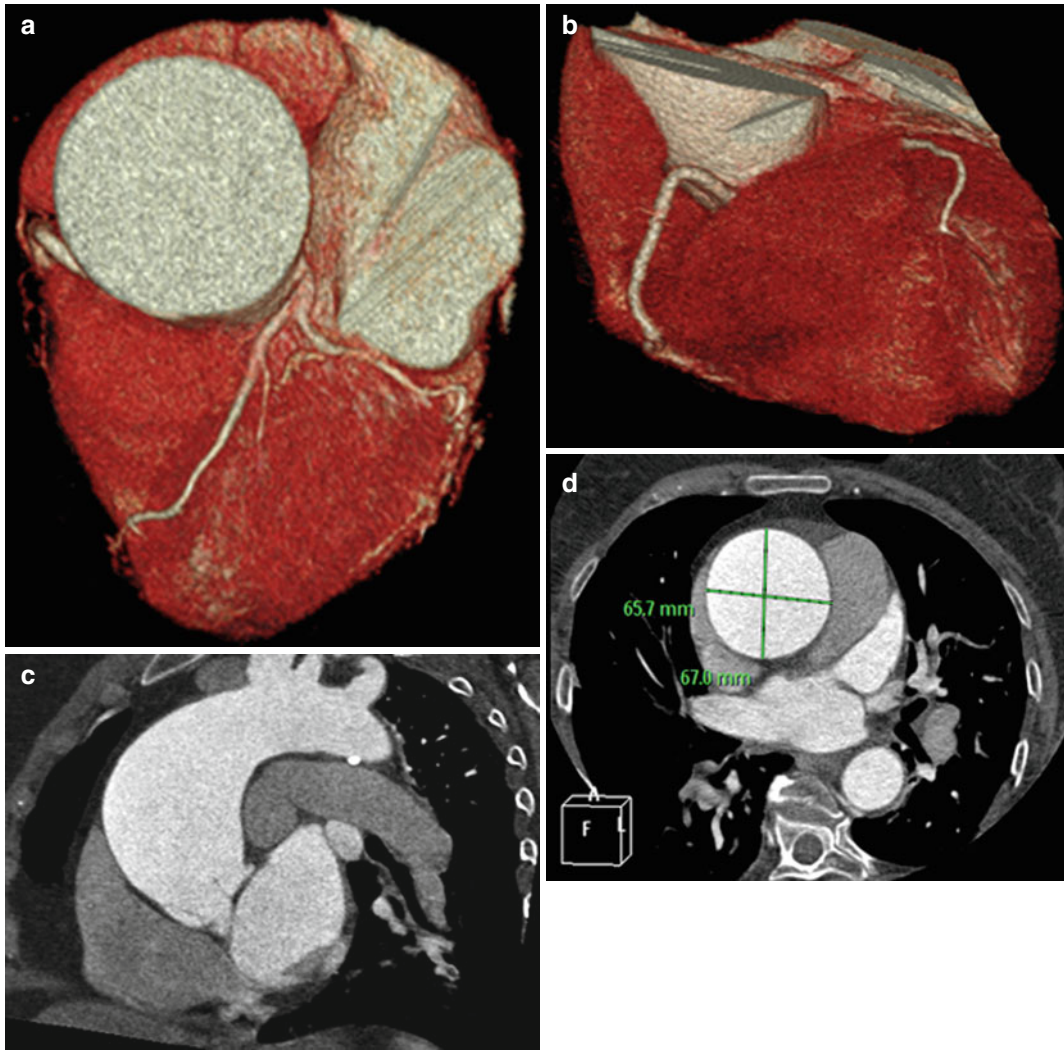

Fig. 12.18 A 70-year-old woman with aortic regurgitation. VR (**a**, **b**) and MPR images (**c**, **d**) display associated ascending aorta dilation

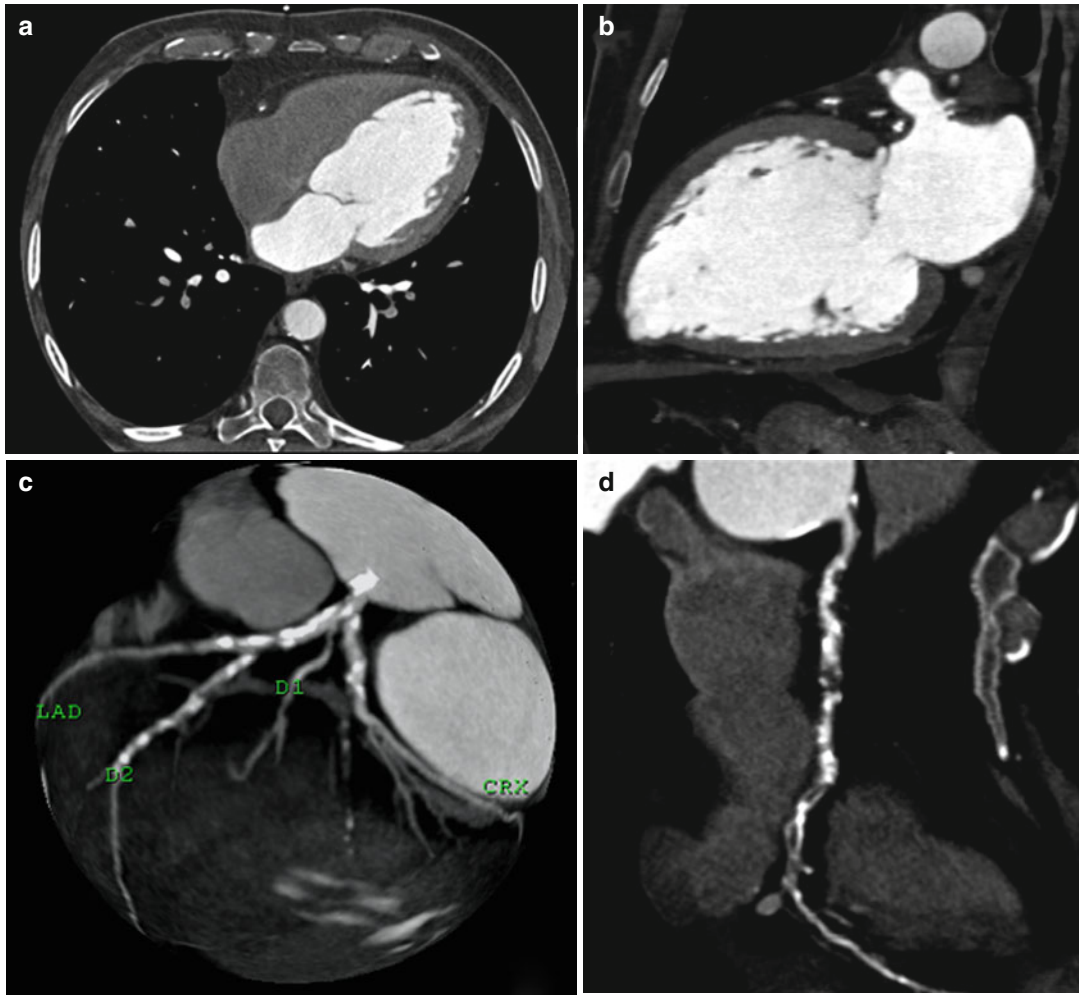

Fig. 12.19 A 72-year-old man with mitral regurgitation and post-ischemic dilated cardiomyopathy. MPR images display the thinning of the left ventricle walls (**a**, **b**) and significant atherosclerosis of the left anterior descending artery (LAD), first diagonal branch (D1), second diagonal branch (D2), circumflex artery (CRX) (**c**) and right coronary arteries (**d**)

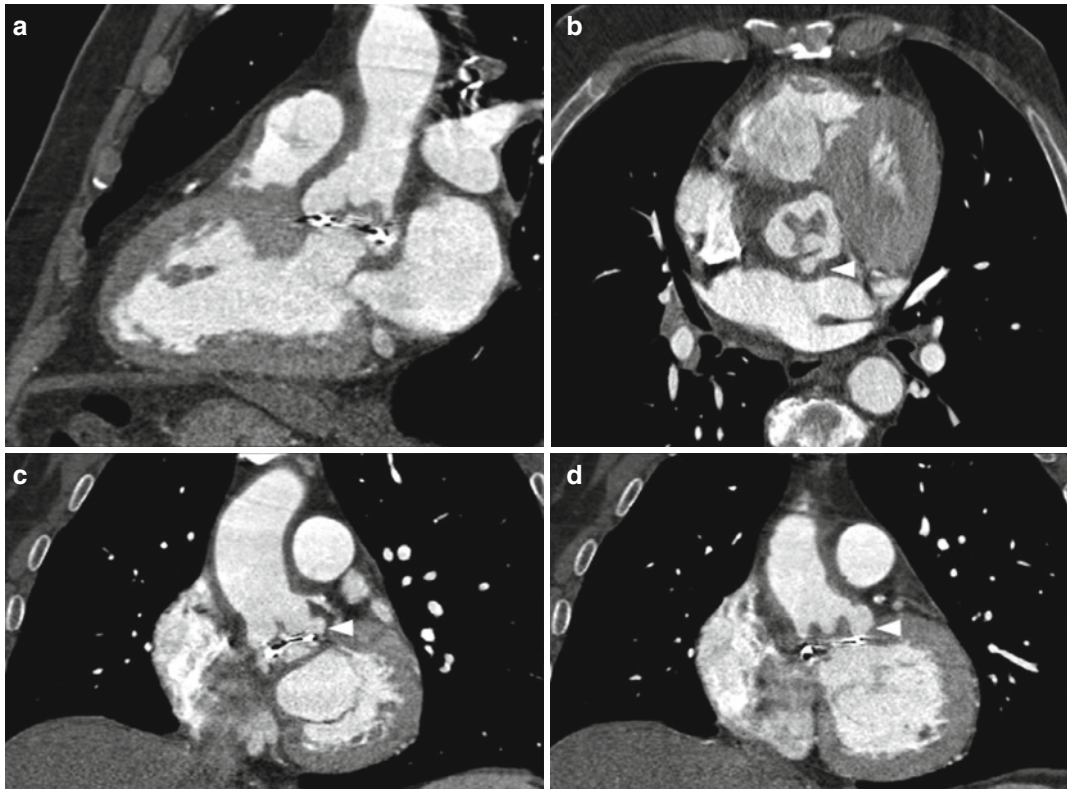

Fig. 12.20 A 72-year-old man with aortic valve replacement complications. CT depicts the thickening of valve leaflets (**a**, **b**) due to endocarditis and periprosthetic leaks (*white head arrows*, **b**–**d**)

References

Abbara S, Pena AJ, Maurovich-Horvat P et al (2007) Feasibility and optimization of aortic valve planimetry with MDCT. AJR Am J Roentgenol 188:356–360

Abbara S, Arbab-Zadeh A, Callister TQ et al (2009) SCCT guidelines for performance of coronary computed tomographic angiography: a report of the Society of Cardiovascular Computed Tomography Guidelines Committee. J Cardiovasc Comput Tomogr 3:190–204

Alegret JM, Duran I, Palazon O et al (2003) Prevalence of and predictors of bicuspid aortic valves in patients with dilated aortic roots. Am J Cardiol 91:619–622

Angelini P, Velasco JA, Flamm S (2002) Coronary anomalies: incidence, pathophysiology, and clinical relevance. Circulation 105:2449–2454

Aurigemma GP, Silver KH, McLaughlin M et al (1994) Impact of chamber geometry and gender on left ventricular systolic function in patients >60 years of age with aortic stenosis. Am J Cardiol 74:794–798

Bache RJ, Vrobel TR, Ring WS et al (1981) Regional myocardial blood flow during exercise in dogs with chronic left ventricular hypertrophy. Circ Res 48:76–87

Basso C, Boschello M, Perrone C et al (2004) An echocardiographic survey of primary school children for bicuspid aortic valve. Am J Cardiol 93:661–663

Bogaert J, Dymarkowski S, Taylor AM (2005) Clinical cardiac MRI. Springer, Berlin/Heidelberg/New York

Bonow RO, Carabello BA, Chatterjee K et al (2006) ACC/AHA 2006 guidelines for the management of patients with valvular heart disease: a report of the American College of Cardiology/American Heart Association Task Force on Practice Guidelines (writing Committee to Revise the 1998 guidelines for the management of patients with valvular heart disease) developed in collaboration with the Society of Cardiovascular Anesthesiologists endorsed by the Society for Cardiovascular Angiography and Interventions and the Society of Thoracic Surgeons. J Am Coll Cardiol 48:e1–e148

Bonow RO, Carabello BA, Chatterjee K et al (2008) 2008 Focused update incorporated into the ACC/AHA 2006 guidelines for the management of patients with valvular heart disease: a report of the American College of Cardiology/American Heart Association Task Force on Practice Guidelines (Writing Committee to Revise the 1998 Guidelines for the Management of Patients

With Valvular Heart Disease): endorsed by the Society of Cardiovascular Anesthesiologists, Society for Cardiovascular Angiography and Interventions, and Society of Thoracic Surgeons. Circulation 118:e523–e661

Brickner ME, Hillis LD, Lange RA (2000) Congenital heart disease in adults: first of two parts. N Engl J Med 342:256–263

Cademartiri F, Malagò R, La Grutta L et al (2007) Coronary variants and anomalies: methodology of visualisation with 64-slice CT and prevalence in 202 consecutive patients. Radiol Med 112:1117–1131

Cademartiri F, La Grutta L, Malagò R et al (2008) Prevalence of anatomical variants and coronary anomalies in 543 consecutive patients studied with 64-slice CT coronary angiography. Eur Radiol 18:781–791

Chan KM, Wage R, Symmonds K et al (2008) Towards comprehensive assessment of mitral regurgitation using cardiovascular magnetic resonance. J Cardiovasc Magn Reson 10:61

Chatzimavroudis GP, Walker PG, Oshinski JN et al (1997) Slice location dependence of aortic regurgitation measurements with MR phase velocity mapping. Magn Reson Med 37:545–551

Cheitlin MD, Armstrong WF, Aurigemma GP et al (2003) ACC/AHA/ASE 2003 guideline update for the clinical application of echocardiography: summary article: a report of the American College of Cardiology/American Heart Association Task Force on Practice Guidelines (ACC/AHA/ASE Committee to Update the 1997 Guidelines for the Clinical Application of Echocardiography). Circulation 108:1146–1162

Chen JJ, Manning MA, Frazier AA et al (2009) CT angiography of the cardiac valves: normal, diseased, and postoperative appearances. Radiographics 29: 1393–1412

Chung R, Zidan M, Henein MY (2008) One stop cardiac investigation 'CT or echocardiography': beyond ejection fraction. Int J Cardiovasc Imaging 24:327–329

Ciotti GR, Vlahos AP, Silverman NH (2006) Morphology and function of the bicuspid aortic valve with and without coarctation of the aorta in the young. Am J Cardiol 98:1096–1102

Dauterman KW, Michaels AD, Ports TA (2003) Is there any indication for aortic valvuloplasty in the elderly? Am J Geriatr Cardiol 12:190–196

Debl K, Djavidani B, Buchner S et al (2006) Delayed hyperenhancement in magnetic resonance imaging of left ventricular hypertrophy caused by aortic stenosis and hypertrophic cardiomyopathy: visualisation of focal fibrosis. Heart 92:1447–1451

Enriquez-Sarano M, Basmadjian AJ, Rossi A et al (1999) Progression of mitral regurgitation: a prospective Doppler echocardiographic study. J Am Coll Cardiol 34:1137–1144

Feuchtner GM, Dichtl W, Friedrich GJ et al (2006a) Multislice computed tomography for detection of patients with aortic valve stenosis and quantification of severity. J Am Coll Cardiol 47:1410–1417

Feuchtner GM, Dichtl W, Schachner T et al (2006b) Diagnostic performance of MDCT for detecting aortic valve regurgitation. AJR Am J Roentgenol 186: 1676–1681

Fieno DS, Kim RJ, Chen EL et al (2000) Contrast-enhanced magnetic resonance imaging of myocardium at risk: distinction between reversible and irreversible injury throughout infarct healing. J Am Coll Cardiol 36:1985–1991

Freed LA, Benjamin EJ, Levy D et al (2002) Mitral valve prolapse in the general population: the benign nature of echocardiographic features in the Framingham Heart Study. J Am Coll Cardiol 40:1298–1304

Fuster V, Rydén LE, Cannom DS et al (2006) ACC/AHA/ESC 2006 guidelines for the management of patients with atrial fibrillation-executive summary: a report of the American College of Cardiology/American Heart Association Task Force on Practice Guidelines and the European Society of Cardiology Committee for Practice Guidelines (Writing Committee to Revise the 2001 Guidelines for the Management of Patients With Atrial Fibrillation): developed in Collaboration With the European Heart Rhythm Association and the Heart Rhythm Society. Circulation 114:e257–e354

Garcia J, Kadem L, Larose E et al (2011) Comparison between cardiovascular magnetic resonance and transthoracic Doppler echocardiography for the estimation of effective orifice area in aortic stenosis. J Cardiovasc Magn Reson 13:25

Gelfand EV, Hughes S, Hauser TH et al (2006) Severity of mitral and aortic regurgitation as assessed by cardiovascular magnetic resonance: optimizing correlation with Doppler echocardiography. J Cardiovasc Magn Reson 8:503–507

Gilkeson RC, Markowitz AH, Balgude A, Sachs PB (2006) MDCT evaluation of aortic valvular disease. AJR Am J Roentgenol 186:350–360

Globits S, Higgins CB (1995) Assessment of valvular heart disease by magnetic resonance imaging. Am Heart J 129:369–381

Habets J, Symersky P, van Herwerden LA et al (2011) Prosthetic heart valve assessment with multidetector-row CT: imaging characteristics of 91 valves in 83 patients. Eur Radiol 21:1390–1396

Heidenreich PA, Steffens JC, Fujita N et al (1995) The evaluation of mitral stenosis with velocity-encoded cine MRI. Am J Cardiol 75:365–369

Hickey AJ, Wilcken DE, Wright JS, Warren BA (1985) Primary (spontaneous) chordal rupture: relation to myxomatous valve disease and mitral valve prolapse. J Am Coll Cardiol 5:1341–1346

Higgins CB, Sakuma H (1996) Heart disease: functional evaluation with MR imaging. Radiology 199: 307–315

Hoffman JI, Kaplan S (2002) The incidence of congenital heart disease. J Am Coll Cardiol 39:1890–1900

John AS, Dill T, Brandt RR et al (2003) Magnetic resonance to assess the aortic valve area in aortic stenosis: how does it compare to current diagnostic standards? J Am Coll Cardiol 42:519–526

Karamitsos TD, Myerson SG (2011) The role of cardiovascular magnetic resonance in the evaluation of valve disease. Prog Cardiovasc Dis 54:276–286

Kon MW, Myerson SG, Moat NE et al (2004) Quantification of regurgitant fraction in mitral regurgitation by cardiovascular magnetic resonance: comparison of techniques. J Heart Valve Dis 13:600–607

Koos R, Kuhl HP, Muhlenbruch G et al (2006) Prevalence and clinical importance of aortic valve calcification detected incidentally on CT scans: comparison with echocardiography. Radiology 241:76–82

Kramer CM, Barkhausen J, Flamm SD et al (2008) Standardized cardiovascular magnetic resonance imaging (CMR) protocols, society for cardiovascular magnetic resonance: board of trustees task force on standardized protocols. J Cardiovasc Magn Reson 10:35

Krayenbuehl HP, Hess OM, Ritter M et al (1988) Left ventricular systolic function in aortic stenosis. Eur Heart J 9(Suppl E):19–23

Lin SJ, Brown PA, Watkins MP et al (2004) Quantification of stenotic mitral valve area with magnetic resonance imaging and comparison with Doppler ultrasound. J Am Coll Cardiol 44:133–137

Lombardi M, Bartolozzi C (2004) MRI of the heart and vessels. Springer, Milan

Mahabadi AA, Achenbach S, Burgstahler C et al (2010) Safety, efficacy, and indications of beta-adrenergic receptor blockade to reduce heart rate prior to coronary CT angiography. Radiology 257:614–623

Mahle WT, Parks WJ, Fyfe DA et al (2003) Tricuspid regurgitation in patients with repaired Tetralogy of Fallot and its relation to right ventricular dilatation. Am J Cardiol 92:643–645

Manghat NE, Rachapalli V, Van Lingen R et al (2008) Imaging the heart valves using ECG-gated 64-detector row cardiac CT. Br J Radiol 81:275–290

Meijboom WB, Mollet NR, Van Mieghem CA et al (2006) Pre-operative computed tomography coronary angiography to detect significant coronary artery disease in patients referred for cardiac valve surgery. J Am Coll Cardiol 48:1658–1665

Messika-Zeitoun D, Serfaty JM, Laissy JP et al (2006) Assessment of the mitral valve area in patients with mitral stenosis by multislice computed tomography. J Am Coll Cardiol 48:411–413

Myerson SG, Francis JM, Neubauer S (2010) Direct and indirect quantification of mitral regurgitation with cardiovascular magnetic resonance, and the effect of heart rate variability. MAGMA 23:243–249

Nitenberg A, Foult JM, Antony I et al (1988) Coronary flow and resistance reserve in patients with chronic aortic regurgitation, angina pectoris and normal coronary arteries. J Am Coll Cardiol 11:478–486

Nkomo VT, Gardin JM, Skelton TN et al (2006) Burden of valvular heart diseases: a population-based study. Lancet 368:1005–1011

Otto C, Lind B, Kitzman D et al (1999) Association of aortic-valve sclerosis with cardiovascular mortality and morbidity in the elderly. N Engl J Med 341:142–147

Owens DS, Katz R, Takasu J et al (2010) Incidence and progression of aortic valve calcium in the Multi-ethnic Study of Atherosclerosis (MESA). Am J Cardiol 105:701–708

Pohle K, Mäffert R, Ropers D et al (2001) Progression of aortic valve calcification: association with coronary atherosclerosis and cardiovascular risk factors. Circulation 104:1927–1932

Raman SV, Shah M, McCarthy B et al (2006) Multi-detector row cardiac computed tomography accurately quantifies right and left ventricular size and function compared with cardiac magnetic resonance. Am Heart J 151:736–744

Ranganathan N, Lam JH, Wigle ED, Silver MD (1970) Morphology of the human mitral valve. II. The value leaflets. Circulation 41:459–467

Rivera JM, Vandervoort PM, Vazquez de Prada JA et al (1993) Which physical factors determine tricuspid regurgitation jet area in the clinical setting? Am J Cardiol 72:1305–1309

Roger VL, Go AS, Lloyd-Jones DM et al (2011) Heart disease and stroke statistics – 2011 update: a report from the American Heart Association. Circulation 123:e18–e209

Sagie A, Freitas N, Padial LR et al (1996) Doppler echocardiographic assessment of long-term progression of mitral stenosis in 103 patients: valve area and right heart disease. J Am Coll Cardiol 28:472–479

Sandstede JJW, Beer M, Hofmann S et al (2000) Changes in left and right ventricular cardiac function after valve replacement for aortic stenosis determined by cine MR imaging. J Magn Reson Imaging 12:240–246

Sato T, Anno H, Kondo T et al (2005) Applicability of ECG-gated multislice helical ct to patients with atrial fibrillation. Circ J 69:1068–1073

Simonetti OP, Kim RJ, Fieno DS et al (2001) An improved MR imaging technique for the visualization of myocardial infarction. Radiology 218:215–223

Stewart BF, Siscovick D, Lind BK et al (1997) Clinical factors associated with calcific aortic valve disease: Cardiovascular Health Study. J Am Coll Cardiol 29:630–634

Taylor AJ, Cerqueira M, Hodgson JM et al (2010) ACCF/SCCT/ACR/AHA/ASE/ASNC/NASCI/SCAI/SCMR 2010 appropriate use criteria for cardiac computed tomography. A report of the American College of Cardiology Foundation Appropriate Use Criteria Task Force, the Society of Cardiovascular Computed Tomography, the American College of Radiology, the American Heart Association, the American Society of Echocardiography, the American Society of Nuclear Cardiology, the North American Society for Cardiovascular Imaging, the Society for Cardiovascular Angiography and Interventions, and the Society for Cardiovascular Magnetic Resonance. J Am Coll Cardiol 56:1864–1894

Tzemos N, Therrien J, Yip J et al (2008) Outcomes in adults with bicuspid aortic valves. JAMA 300:1317–1325

Vahanian A, Baumgartner H, Bax J et al (2007) Guidelines on the management of valvular heart disease: the Task Force on the Management of Valvular Heart Disease of the European Society of Cardiology. Eur Heart J 28:230–268

Willmann JK, Weishaupt D, Lachat M et al (2002) Electrocardiographically gated multi–detector row CT for assessment of valvular morphology and calcification in aortic stenosis. Radiology 225:120–128